Experimental validation of acoustic radiation force induced shear wave interference patterns

2012 Phys. Med. Biol. 57 21

(http://iopscience.iop.org/0031-9155/57/1/21)

Phys. Med. Biol. **57** (2012) 21–30 doi:10.1088/0031-9155/57/1/21

Experimental validation of acoustic radiation force induced shear wave interference patterns

Kenneth Hoyt[1,2,3], Zaegyoo Hah[4], Chris Hazard[5] and Kevin J Parker[4]

[1] Department of Radiology, University of Alabama at Birmingham, Birmingham, AL 35294, USA
[2] Department of Biomedical Engineering, University of Alabama at Birmingham, Birmingham, AL 35294, USA
[3] Comprehensive Cancer Center, University of Alabama at Birmingham, Birmingham, AL 35294, USA
[4] Department of Electrical and Computer Engineering, University of Rochester, Rochester, NY 14627, USA
[5] General Electric Global Research, Niskayuna, NY 12309, USA

E-mail: hoyt@uab.edu

Received 14 July 2011, in final form 28 September 2011
Published 29 November 2011
Online at stacks.iop.org/PMB/57/21

Abstract

A novel elasticity imaging system founded on the use of acoustic radiation forces from a dual beam arrangement to generate shear wave interference patterns is described. Acquired pulse-echo data and correlation-based techniques were used to estimate the resultant deformation and to visualize tissue viscoelastic response. The use of normal versus axicon focal configurations was investigated for effects on shear wave generation. Theoretical models were introduced and shown in simulation to accurately predict shear wave propagation and interference pattern properties. In a tissue-mimicking phantom, experimental results are in congruence with theoretical predictions. Using dynamic acoustic radiation force excitation, results confirm that shear wave interference patterns can be produced remotely in a particular tissue region of interest (ROI). Overall, preliminary results are encouraging and the system described may prove feasible for interrogating the viscoelastic properties of normal and diseased tissue types.

(Some figures in this article are in colour only in the electronic version)

1. Introduction

The field of ultrasound-based elasticity imaging has evolved considerably over the last decade. The generalized premise behind all elasticity imaging techniques is to apply a mechanical stimulus to the target tissue and then image the deformation response. As detailed in a recent review, early innovations were focused around externally applied static or dynamic compression-based strategies, while more recent developments have transitioned to using acoustic radiation forces to remotely induce tissue motion prior to elastic property estimation

(Parker *et al* 2011). Limitations aside, these latter methods might prove advantageous from a clinical perspective. They permit elasticity imaging of a broader array of tissues and organs while not being limited to superficial structures, which is typically the case for externally applied deformation-based elasticity imaging techniques.

It has been shown that a pair of dynamic mechanical sources vibrating at slightly offset frequencies could induce propagating shear waves that constructively combine to create slowly propagating interference patterns (Wu *et al* 2004). An analysis of shear wave interference patterns permits the estimation of the spatial elastic properties, namely, shear wave speed distributions (Wu *et al* 2006, Hoyt *et al* 2007, 2008a). Furthermore, the collection of shear wave interference pattern image sequences for a range of vibration frequencies allows quantification of tissue viscoelastic properties (Hoyt *et al* 2008c). Changes in these tissue viscoelastic properties are intimately linked to several diseased tissue types such as cancerous tumors (Hoyt *et al* 2008b).

In a more recent development, the theoretical analysis of shear wave interference patterns by means of dynamic acoustic radiation forces was presented (Hoyt 2011). In parallel, it was demonstrated that acoustic radiation forces from a spatially separated pair of single element transducers were sufficient to create shear wave interference patterns in tissue mimicking phantoms (Hah *et al* 2010). While pulse-echo data were collected using a modified commercial ultrasound system for elasticity image formation, the acoustic radiation force sources were external components. Use of external sources may limit clinical translation due to setup complexity and inherent problems related to ensuring that the radiation force source pair bisects the same image plane as the shear wave motion tracking system.

In this paper, we detail an integrated ultrasound system that both induces tissue deformation using acoustic radiation forces and subsequently tracks shear wave propagation using correlation-based methods. An analysis of normal and axicon focusing of acoustic radiation force sources is presented to investigate effects on shear wave interference patterns. Experimental results from the tissue-mimicking phantom are compared to numerical simulations based on a Green's function formalism.

2. Simulation methods

Simulations were programmed using the software package Matlab (Mathworks, Natick, MA, USA). As detailed previously by (Hoyt *et al* 2011), the general strategy was to analytically compute acoustic radiation force-induced tissue displacements using a Green's function analysis and then superimpose these displacement fields onto ultrasound backscattered signals for each time step of shear wave propagation. Correlation-based speckle tracking techniques allow displacement estimation resulting from the propagation of shear waves. Collectively, this approach mimics an ultrasound system that both induces and tracks shear wave motion.

The linear acoustic Matlab-based modeling program known as FIELD II (Jensen and Svendsen 1992) independently simulated both high-intensity ultrasound pulse transmissions and low-intensity backscattered echo fields (i.e. RF lines) describing conventional B-mode imaging. The former sequence is used to induce tissue motion, while the latter sequence is processed to track shear wave propagation across the image plane relative to a reference field. For both configurations described, the transducer was modeled as a 128 element linear array (0.3 mm pitch) with a 5 MHz center frequency.

As shown in figure 1, a dual-beam (separation distance d of 18 mm) displacement-inducing transducer configuration was simulated at a focal depth f_L of 25 mm and for a given f-number defined as $F\# = f_L/a$, where a is the effective aperture size defined by the number of active elements. Ultrasound beams for remotely inducing shear wave propagation

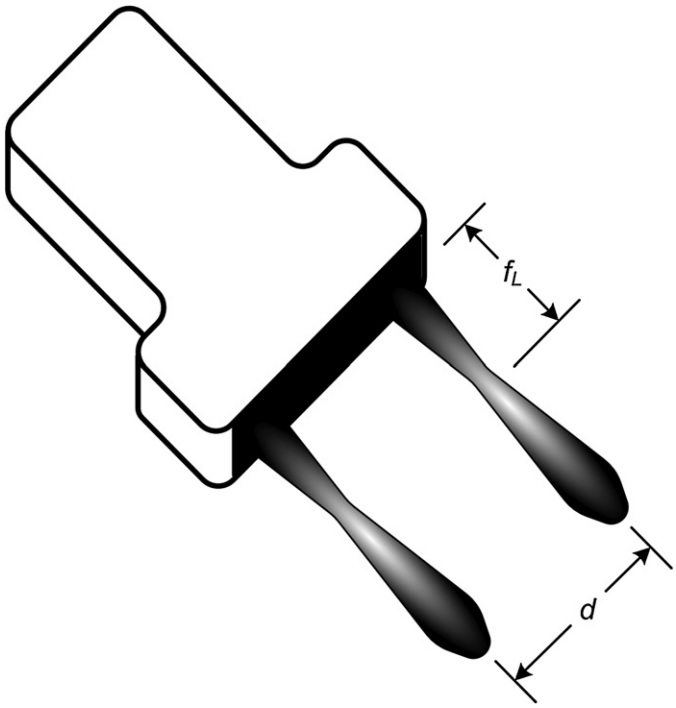

Figure 1. Illustration of ultrasound imaging transducer for and vector orientation excitation of crawling wave patterns using acoustic radiation forces. At a focal depth of f_L, pulsing of two ultrasound beams (separated by distance d) establish propagating shear waves due to acoustic radiation forces that combine to form a shear wave interference pattern. Conventional ultrasound imaging sequences track shear wave displacements within the image plane.

at depth were focused either using normal or axicon techniques, figure 2. Note that imaging regions of interest (ROIs) were confined to 18 mm of width and 10–37 mm in depth to mimic experimental system conditions. Given a 0.25 ms tone burst (1250 cycles at 5 MHz), intensities were normalized to a time-average intensity value of 1000 W cm^{-2} to reflect relevant radiation force conditions (Palmeri *et al* 2005). After normalizing radiation force distributions by area under the curve techniques, tissue displacement fields were computed (Hoyt *et al* 2011).

A uniform isoechoic scattering phantom containing randomly positioned point targets (density of 10 per mm^2) was simulated again using FIELD II. Initial scatterer locations represent pre-displacement (reference) positions, while displacements determined via viscoelastic Green's function analysis were used to reposition the scatterers and reflect shear wave motion following acoustic radiation force excitation. Image frame rates were set to 2.5 kHz and scatterer repositions for each RF line were numerically computed for each time step using shape-preserving piecewise cubic interpolation along the beam axis. Acoustic radiation forces and subsequent tissue displacements were independently simulated throughout the ROI for each of the two pushing beams. Shear wave interference patterns were then synthesized by assuming a 500 Hz pulse repetition frequency and superimposition of delayed (2 ms) displacement fields. This synthesis from only two properly spaced pushing pulses produces a steady-state shear wave interference pattern image while minimizing lengthy pulsing sequences which renders implementation on an actual ultrasound system problematic.

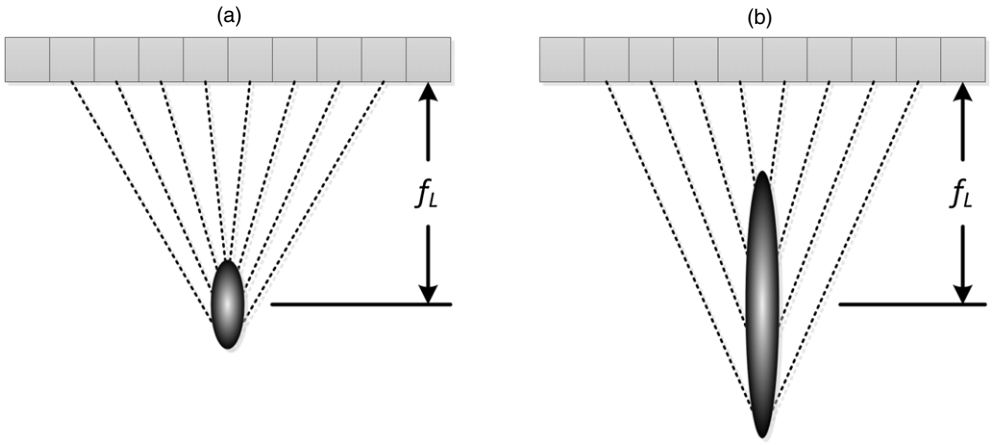

Figure 2. Description of ultrasound beams for remotely inducing shear wave propagation at depth for (a) normal and (b) axicon focal configurations.

For a temporal series of simulated ultrasound images, a cosine curve was fit to each time vector using nonlinear least-squares regression techniques to combat any image noise concerns (particularly for matched experimental results). Using a one-dimensional 20-sample kernel, axial motion was then estimated as the peak position of a cross-correlation function applied to congruent pre- and post-displacement RF data segments. Subsample interpolation using a parabolic function was employed to improve displacement estimation accuracy (Cespedes *et al* 1995). One sample kernel shifting allowed displacement estimation as a function of depth and for each simulated RF data sequence. The standard deviation at each spatial location was computed and imaged to illustrate shear wave interference patterns.

3. Experimental methods

A modified GE Logiq 9 ultrasound system (GE Medical Systems, Milwaukee, WI, USA) equipped with a dedicated 5 MHz transrectal transducer was employed for both inducing and tracking shear wave propagation. Although the maximum active aperture was 26 mm, image ROIs were confined to an 18 mm lateral width at depths of 10–37 mm. For RF lines separated by 0.6 mm, this equated to 31 data sequences in the lateral dimension. Ultrasound beams for acoustic radiation force induction of shear wave propagation were focused at a depth of 25 mm (using either normal or axicon focal configurations) and located on the extreme edges of the imaging ROI. Output intensity values (I_{SPTA}) for the acoustic radiation force pulse sequences were measured to be 1.6 and 0.5 W cm^{-2} for normal and axicon focusing, respectively.

Custom scanner imaging sequences were developed to permit shear wave generation and subsequent tracking. As illustrated in figure 3, the process begins with the system acquiring a reference RF data sequence and then a high-intensity ultrasound tone burst (0.25 ms) induces shear wave propagation. Following a 0.5 ms delay to minimize reverberation artifacts, 48 additional RF data sequences are collected along the same line of sight at a rate of 2.5 kHz (akin to pulse Doppler methods). After a short delay for duty cycle maintenance, this process is repeated (alternating between left and right pushing beams to minimize heating effects) until all 31 data sequences (lateral vectors) in the ROI are populated. For the ROI size chosen, the complete imaging sequence required an elapsed time of 2.4 s. Tissue displacement maps and shear wave interference patterns were then synthesized (at a rate of 500 Hz) from the

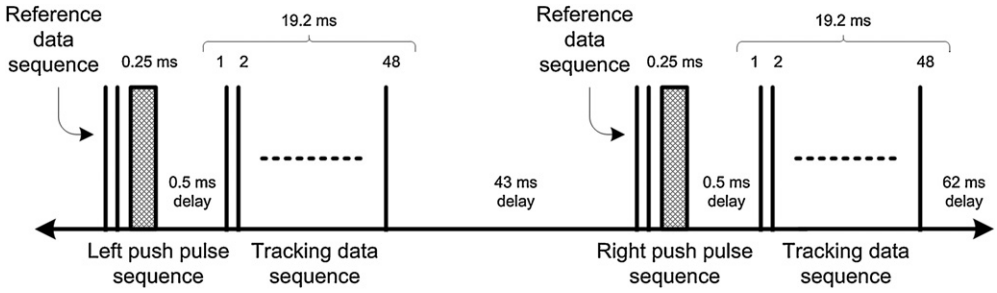

Figure 3. Time diagram illustrating the scan sequence of the ultrasound system. After acquiring a reference RF line sequence, a high-intensity tone burst induces shear wave propagation. Tracking data sequences are then collected at a rate of 2.5 kHz for a particular line of sight. This process is repeated for left and right pushing beams until all RF data vector sequences are populated for each lateral location along the ROI.

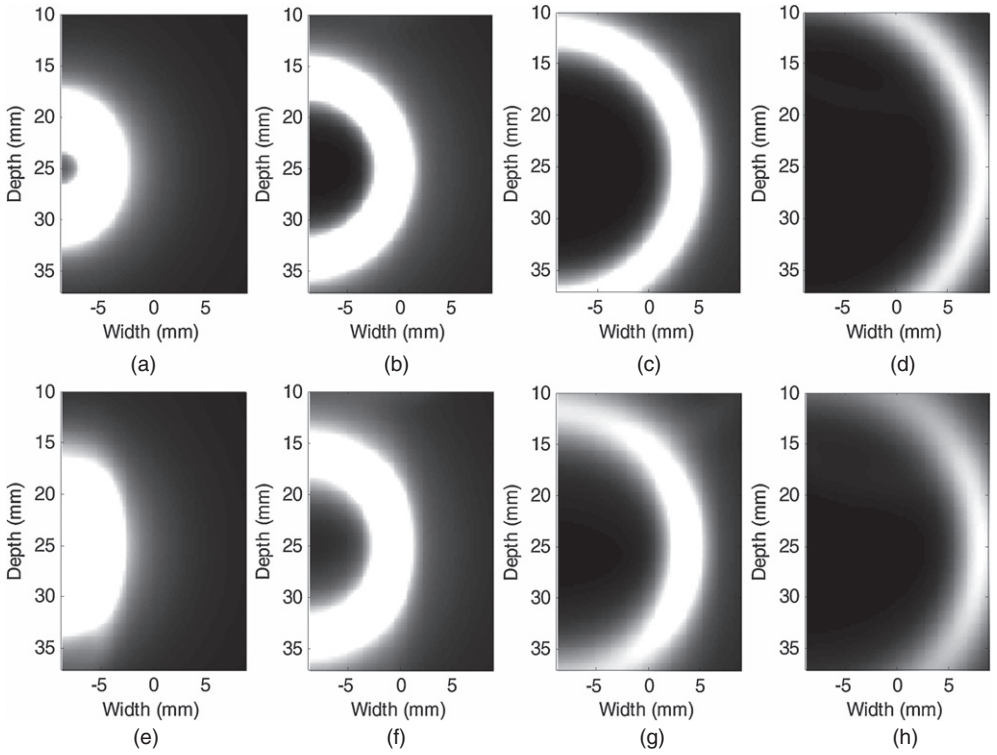

Figure 4. Simulated propagating shear waves at a depth of 25 mm for normal (top) and axicon (bottom) focal configurations. After initial displacement, images depict attenuating shear waves at time points of ((a) and (e)) 1.3, ((b) and (f)) 2.5, ((c) and (g)) 3.7 and ((d) and (h)) 4.9 ms.

left and right pushing beams and filtered using the computational techniques described in section 2.

Validation experiments were conducted using a gelatin-based tissue-mimicking phantom. Briefly, a solution of 184 g of gelatin (Gelatin Innovations Inc, Schiller Park, IL, USA), 2.7 g of agar (Bector and Dickinson, Sparks, MD, USA) and 16.2 g of sodium chloride (Fisher

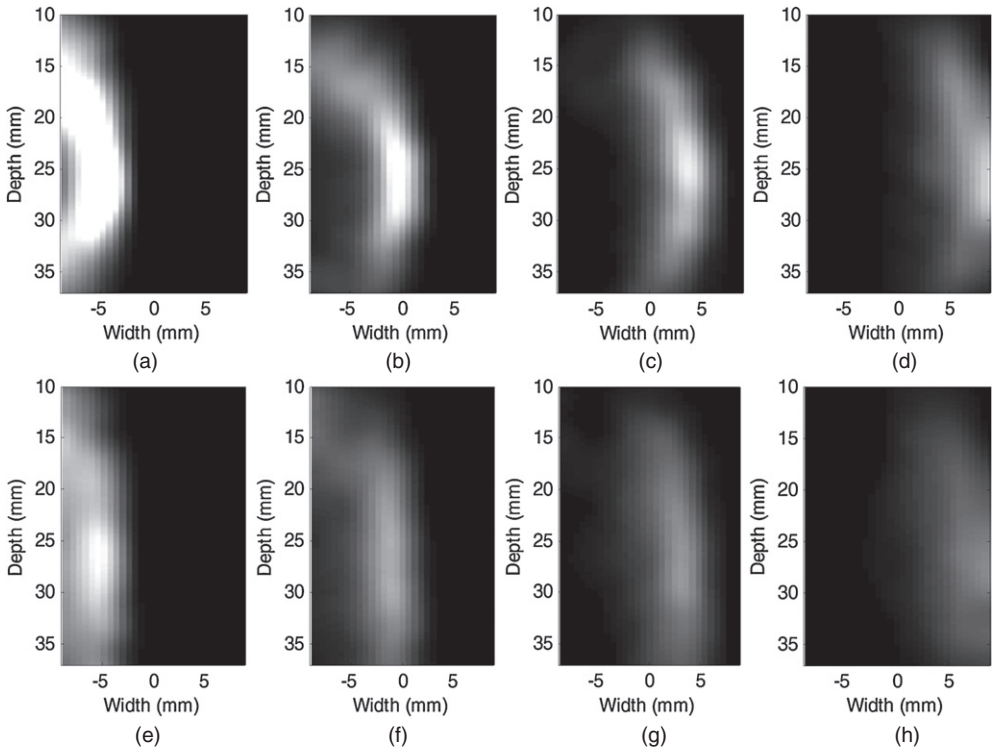

Figure 5. Experimental propagating shear waves at a depth of 25 mm for normal (top) and axicon (bottom) focal configurations. After initial displacement, images depict attenuating shear waves at time points of ((a) and (e)) 1.3, ((b) and (f)) 2.5, ((c) and (g)) 3.7 and ((d) and (h)) 4.9 ms.

Scientific, Fair Lawn, NJ, USA) was heated to 90 °C to produce a homogeneous gel. The mixture was then allowed to cool to 30 °C (near the congealing point) before pouring into a cylindrical-shaped mold (12 cm depth). Molds were subsequently stored in a cold room (5 °C) for 24 h to ensure that the gel congealed. It was assumed that the final phantom product had acoustic properties similar to human tissue.

4. Results

Generation of shear waves in a viscoelastic medium owing to a single focused ultrasound beam (depth of 25 mm) was simulated. As figure 4 details, after initial displacement, attenuating shear waves propagate away from the acoustic focus at a rate equal to the shear wave speed of the supporting medium (3.6 m s^{-1}). Comparison of images produced using normal (figures 4(a)–(d)) or axicon (figures 4(e)–(h)) focusing concludes that the former induces a spherically propagating shear wave with uniform attenuation at a distance. While the shear waves induced using axicon focal characteristics also exhibit notable attenuation, the effect is less pronounced in the transverse direction. Since axicon focusing distributes the ultrasound beam energy over a larger elongated spatial area (compared to normal focusing), propagating shear waves become slightly more planar along the wave fronts positioned at the same depth. Matched experimental elasticity results for a single focused ultrasound beam are presented in figure 5. Analogous to simulated findings, attenuated shear waves progressively travel away from the acoustic radiation force sources. Again, a normal focusing

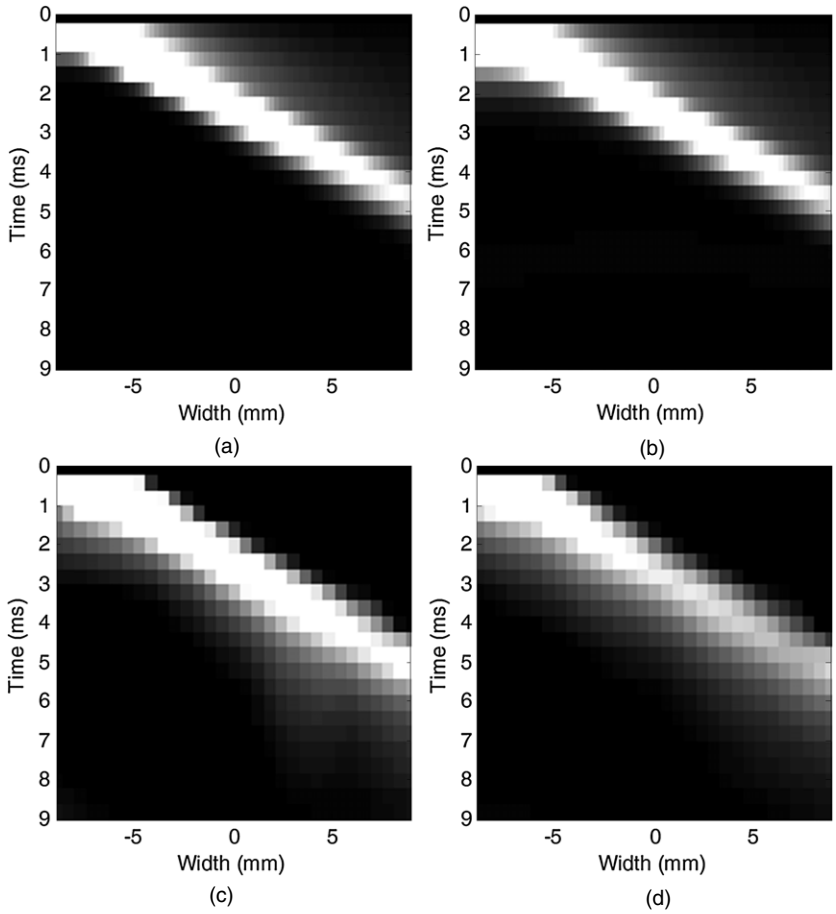

Figure 6. Temporal behavior of a propagating shear wave mapped as a function of the image plane width. Images detail ((a) and (b)) simulated and ((c) and (d)) experimental slow-time shear wave propagation away from the ultrasound beam focal zone located at a depth of 25 mm for both ((a) and (c)) normal and ((b) and (d)) axicon focal configurations.

(figures 5(a)–(d)) configuration produces an apparent spherically propagating shear wave, whereas axicon focusing (figures 5(e)–(h)) yields more planar shear wave fronts. Given that acoustic radiation force induced displacements are of the order of micrometers, displacement estimations can exhibit a low signal-to-noise ratio. The cumulative effect is that current image quality for experimental findings is compromised but encouraging.

Temporal characteristics of acoustical radiation force induced propagating shear waves mapped as a function of the image plane width (from the ultrasound beam focus, 25 mm) are presented in figure 6. The match of theory (figures 6(a) and (b)) to experiment (figures 6(c) and (d)) is reasonable but close inspection reveals some differences. Specifically, experimental shear wave patterns tend to have more variations in the vertical direction and can be slightly wider in the horizontal direction compared with theoretical results. These are likely due to a number of factors, including again the limited signal-to-noise ratio of the displacement measurements and small inaccuracies in the numerical model (e.g. attenuation, beam pattern and dispersion parameters). Notwithstanding, temporal characteristics of the propagating shear waves along the transverse dimension (at focal depth) are comparable for both normal

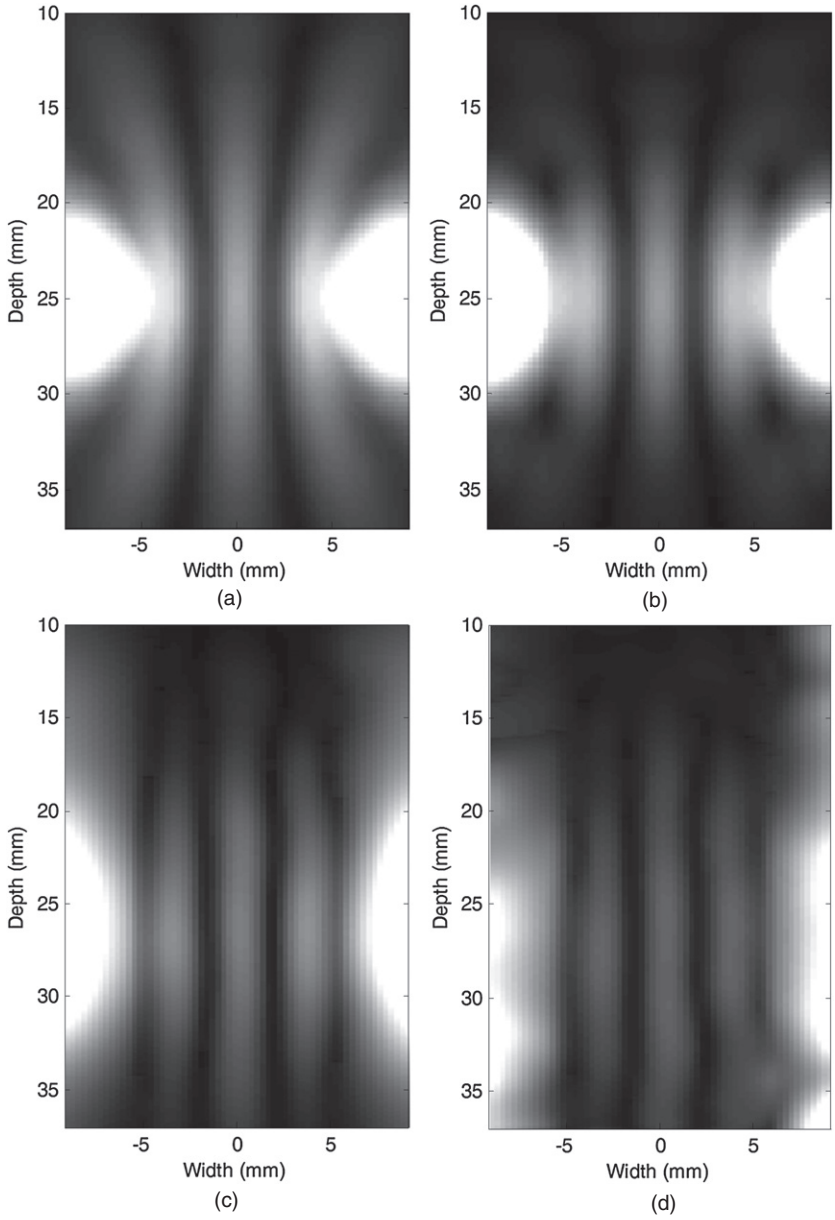

Figure 7. Shear wave interference patterns induced using a pulse repetition frequency of 500 Hz. Images reflect matched ((a) and (b)) simulation and ((c) and (d)) experimental findings for both ((a) and (c)) normal and ((b) and (d)) axicon focal configurations at a depth of 25 mm.

and axicon focal configurations. The analysis of each image reveals that the shear wave speed is about 3.6 m s^{-1}.

Using a pair of spatially separated ultrasound beams, the application of acoustic radiation forces produces shear waves that propagate away from the initial displacement source. By independently tracking displacement fields across the image plane from each source, periodic tissue motion sequences can be realized by delayed superimposition of these same

shear wave displacement fields. Assuming a 500 Hz repetition frequency for each of the acoustic radiation force sources, shear wave interference pattern images were then synthesized, figure 7. Matched simulation (figure 7(a) and (b)) and experimental (figure 7(c) and (d)) shear wave interference pattern images corresponding to either normal or axicon ultrasound beam focusing are presented. Given spatially distributed shear wave interference patterns, the shear wave speed of the supporting medium can be estimated as two times the product of the spatial shear wavelength and repetition frequency (Wu *et al* 2004). For simulated images presented in figure 7, the spatial wavelength at the focal depth was measured to be 3.56 mm, yielding a shear wave speed estimate of 3.56 m s^{-1} and an error of 1.1% from the true shear speed (i.e. 3.6 m s^{-1}). Likewise, shear wave speed estimates derived from the experimental shear wave interference pattern images was found to be approximately 3.51 m s^{-1} and in accord with those computed from figure 5 (error of 2.5%).

Comparison of elasticity images in figure 7 derived using normal versus axicon focusing further reveals that the former produces pattern bands in the far field with discernible spreading and wavelength elongation. If plane wave conditions are vital, then axicon focusing theoretically yields slightly better results albeit differences are not apparent when inspecting experimental shear wave interference pattern images. Future work will investigate the energy dose and thermal effects associated with using both focal configurations for acoustic radiation force excitation of shear wave interference patterns analogous to previous studies (Palmeri and Nightingale 2004).

5. Conclusions

In this paper, generation of shear wave interference patterns using an acoustic radiation force source pair is detailed. Theoretical models were shown in simulation to accurately describe experimental findings, which were acquired via a modified commercial GE Logiq 9 ultrasound system. The role of ultrasound beam focus configuration on radiation force induced shear wave propagation was explored. Although both normal and axicon focusing resulted in quality shear wave interference patterns, axicon-based results can be achieved at a fraction of the acoustic intensity (0.5 W cm^{-2} versus 1.6 W cm^{-2} for normal focusing). Given an FDA recommendation that ultrasound intensity should not exceed 0.72 W cm^{-2}, axicon focusing falls below this recommended safety level and is an advantage compared to the higher intensity associated with normal focusing.

While the utility of shear wave interference patterns for quantitative estimation of tissue elastic properties has been detailed (Wu *et al* 2006, Hoyt *et al* 2007, 2008a, 2008c, 2008b), there are inherent limitations to shear wave excitation using dynamic mechanical sources (conventional strategy). As shear waves progressively attenuate, the use of external mechanical sources limits the capability of elasticity imaging at depth in biological tissues. While vibrational amplitudes can be increased to improve shear wave penetration, overlying tissues and propagation loss still complicate any quantitative analyses (Hoyt *et al* 2008c). Using acoustic radiation force excitation, shear wave interference patterns can be produced remotely in a particular tissue ROI (Hah *et al* 2010). Due to high absorption properties, the acoustic energy (and thermal dose) required to generate acceptable shear waves interference pattern images in tissue could be large introducing the potential of harmful bioeffects. Additionally, potential limitations of the internal excitation method described include the effective frame rate and ability to generate acceptable interference patterns in complex tissue due to non-planar propagating shear waves from the individual sources. Although displacement amplitudes may be compromised using internal ultrasound-based excitation sources (Nightingale *et al* 2003, Palmeri *et al* 2006), they do offer the promise of interrogating the shear wave speed

properties in a broad range of tissue types while not limiting to superficial structures, which is the case using external mechanical sources. Overall, the experimental validation of acoustic radiation force induced shear wave interference patterns was presented and results warrant further investigation.

Acknowledgment

This research project was supported in part by NIH grant 5RO1AG016317-07.

References

Cespedes EI *et al* 1995 Methods for the estimation of subsample time-delays of digitized echo signals *Ultrason. Imaging* **17** 142–71

Hah Z *et al* 2010 Crawling waves from radiation force excitation *Ultrason. Imaging* **32** 177–189

Hoyt K 2011 Theoretical analysis of shear wave interference patterns by means of dynamic acoustic radiation forces *Int. J. Multiphysics* **1** 9–23

Hoyt K, Castaneda B and Parker K J 2008a Two-dimensional sonoelastographic shear velocity imaging *Ultrasound Med. Biol.* **34** 276–88

Hoyt K *et al* 2008b Tissue elasticity properties as biomarkers for prostate cancer *Cancer Biomarkers* **4** 213–25

Hoyt K *et al* 2008c Quantitative sonoelastography for the *in vivo* assessment of skeletal muscle viscoelasticity *Phys. Med. Biol.* **53** 4063–80

Hoyt K, Parker K J and Rubens D J 2007 Real-time shear velocity imaging using sonoelastographic techniques *Ultrasound Med. Biol.* **33** 1086–97

Jensen J A and Svendsen N B 1992 Calculation of pressure fields from arbitrarily shaped, apodized, and excited ultrasound transducers *IEEE Trans. Ultrason. Ferrorelectr. Freq. Control* **39** 262–7

Nightingale K, McAleavey S and Trahey G 2003 Shear-wave generation using acoustic radiation force: *in vivo* and *ex vivo* results *Ultrasound Med. Biol.* **29** 1715–26

Palmeri M L *et al* 2006 Ultrasonic tracking of acoustic radiation force-induced displacements in homogeneous media *IEEE Trans. Ultrason. Ferroelectr. Freq. Control* **53** 1300–13

Palmeri M L and Nightingale K R 2004 On the thermal effects associated with radiation force imaging of soft tissue *IEEE Trans. Ultrason. Ferroelectr. Freq. Control* **51** 551–65

Palmeri M L *et al* 2005 A finite-element method model of soft tissue response to impulsive acoustic radiation force *IEEE Trans. Ultrason. Ferroelectr. Freq. Control* **52** 1699–712

Parker K J, Doyley M M and Rubens D J 2011 Imaging the elastic properties of tissue: the 20 perspective *Phys. Med. Biol.* **56** 1–29

Wu Z *et al* 2004 Sonoelastographic imaging of interference patterns for estimation of the shear velocity of homogeneous biomaterials *Phys. Med. Biol.* **49** 911–22

Wu Z *et al* 2006 Sonoelastographic imaging of interference patterns for estimation of shear velocity distribution in biomaterials *J. Acoust. Soc. Am.* **120** 535–45